Resonant hole states in a quantum well with semimagnetic barriers

F. V. Kyrychenko
Institute of Physics, Polish Academy of Sciences, Al. Lotników 32/46, 02-668 Warsaw, Poland

Yu. G. Semenov
Institute of Semiconductor Physics, National Academy of Sciences of Ukraine, Prospect Nauki 45, Kiev, 252028, Ukraine.
(Received 8 February 1999)

Theoretical calculations of the valence-band electron states in a two-dimensional quantum well (QW) with diluted magnetic semiconductor barriers are performed in the case of in-plane external magnetic field **B**. Cases of relatively weak and strong magnetic fields should be discriminated. In the first case the barrier continuum spectrum is separated from localized heavy- and light-hole states in a QW. In the case of a strong enough magnetic field, the superimposition of a barrier continuum spectrum on light-hole QW levels can take place due to the giant spin splitting of semimagmetic semiconductor band states. Moreover, the strong mixing between quantum-confined and barrier states takes place due to the nonconservation of angular momentum in an inclined magnetic field. This results in the transformation of light-hole-localized states in a QW to resonant (virtual) ones. We use a Luttinger model with a symmetric rectangular potential to recapture the transition from localized to resonant states with an increasing external magnetic field **B**. Calculations of electron-hole optical transitions show a broadening of optical lines and a shift of their maxima. The considered situation is shown to be easily realized in the structures $Cd_{1-x}Mn_xTe/CdTe/Cd_{1-x}Mn_xTe$. [S0163-1829(99)15231-7]

INTRODUCTION

Use of diluted magnetic semiconductors (DMS's) in two-dimensional (2D) quantum structures is very attractive because it is possible to control the energy parameters of such structures easily by an external magnetic field **B**. This stems from the carrier-magnetic ion-exchange interaction that leads to the effect of giant spin splitting (GSS) of energy bands in DMS's (see Ref. 1).

Typical structures that are investigated in the majority of works look like $Cd_{1-x}Mn_xTe/CdTe/Cd_{1-x}Mn_xTe$, where single (or multiple) CdTe quantum well(s) (QW's) are embedded in DMS barriers. In the case of a zero magnetic field, the electron (hole) band-offset potential $U_{e(h)}$ has to be added to the conduction- (valence-) band Hamiltonian, similar to the case of nonmagnetic 2D semiconductor quantum structures. The magnetic field **B** induces the DMS magnetization **M** which gives rise to the exchange field $\mathbf{G}_{e(h)}$ acting on the electron (e) and hole (h) spins proportionally to the exchange integrals $\alpha(\beta)$ and **M**. If $\mathbf{G}_{e(h)}$ is directed along the growth axis **C** of a quantum structure, it increases the barrier energy for carriers with a certain spin orientation and decreases it for carriers with an opposite orientation. The values of the spin-dependent barrier energy shifts are comparable with band-offset energy shifts U_e and U_h. That is why DMS quantum structures reveal a lot of interesting physical phenomena (see Refs. 2–5).

Due to the degeneracy of the states on the top of the valence band, the hole energy spectrum in such QW structures reveals some peculiarities. Namely due to the confinement effect the valence-band spectrum splits into light-hole (LH) and heavy-hole (HH) subbands. The angular momentum projection on the **C** axis is $M=\pm\frac{1}{2}$ for a LH, and $M=\pm\frac{3}{2}$ for a HH. The magnetic splitting of the barrier states is proportional to the effective spin projection M and equal to $\mp G_h/2$ for the HH states ($M=\pm\frac{3}{2}$), and $\mp G_h/6$ for LH states ($M=\pm\frac{1}{2}$). Among others, the difference between spin splittings of LH and HH states in the barrier can lead to a reversal of a single QW to a single-barrier structure for HH's if the $\pm\frac{3}{2}$ spin shift $G_h/2$ exceeds the height of the potential step U_h, while LH states are still localized in QW's with a depth $U_h-G_h/6$.

This paper draws attention to a qualitatively different situation that appears in the case of an arbitrary orientation of a magnetic field **B**. The exchange interaction is represented by a Zeeman-like term $\mathbf{G}_h\mathbf{J}$, where $\mathbf{G}_h(\mathbf{G}_h\|\mathbf{B})$ is not a scalar potential but an exchange *field* which acts on spin moment. In the case of $\mathbf{B}\|\mathbf{C}$, the system has an axial symmetry, and the projection of the angular momentum on **C** axis is a good quantum number for valence electrons with zero in-plane wave vector. When the vectors **B** and **C** are not collinear, the system loses axial symmetry and $M=\pm\frac{3}{2},\pm\frac{1}{2}$ (the projection of the angular moment on **B**) is no longer good quantum number. In this case the eigenvectors of LH and HH localized states should be represented by a linear combinations of the vectors $|M\rangle$. This modification leads to a drastic revision of the traditional classification of the confinement levels once the barrier states reach and then cross some of the localized QW levels (see Fig. 1). In this case QW discrete states turn out to be inside the barrier continuous spectrum, and acquire their features due to spin mixing by an inclined field $\mathbf{G}_h$. In other words, the localized states in a single QW transform to resonant ones. It should be emphasized that the total angular momentum conservation law forbids such kinds of resonant states in the case of $\mathbf{B}\|\mathbf{C}$.

Contrary to the situation of narrow-gap semiconductor quantum structures, where electron resonant states appear due to **kp** coupling to the bulk valence-band continuum,[6–8] the LH-HH resonant mixing is realized in a strong enough inclined external magnetic field even in the case of a zero in-plane wave vector. Thus we have a good chance to recapture the transition from localized to resonant (or virtual)

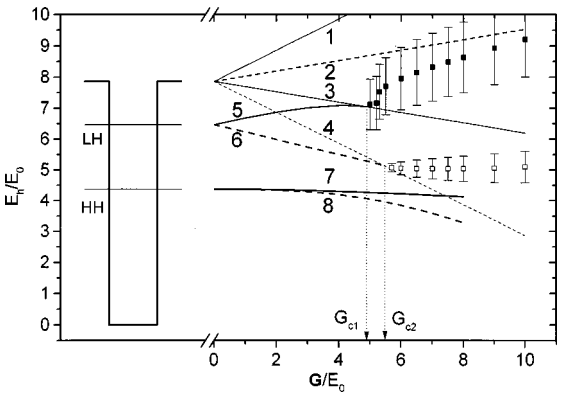

FIG. 1. 20-Å-wide $Cd_{0.88}Mn_{0.12}Te/CdTe/Cd_{0.88}Mn_{0.12}Te$ QW profile with LH and HH energy positions and their spin splitting in the case of $\mathbf{G}\perp\mathbf{C}$ (curves 5–8). Evolutions of the barrier hole states with $J_Z=-\frac{3}{2}$, $-\frac{1}{2}$, $+\frac{1}{2}$, and $+\frac{3}{2}$ far from the QW region correspond to the lines 1–4, respectively. Solid lines represent energy of states which are mixture of $|-\frac{3}{2}\rangle$ and $|+\frac{1}{2}\rangle$ states. Dashed lines correspond to that of $|+\frac{3}{2}\rangle$ and $|-\frac{1}{2}\rangle$ states. Squares represent the energies of states of continuous spectrum with maximum values of probability to find a hole in the QW region (see Fig. 2), bars represent the FWHM (full width at half maximum) of the curves similar to those in Fig. 2. The exchange fields G_{c1} and G_{c2} mark the crossing of barrier and LH energy branches with non-orthogonal states.

states in a QW with semimagnetic barriers by changing the magnetic field *B*.

In the following section we develop the theory of localized hole states in a QW with DMS barriers. For simplicity we limit ourselves to the case of $\mathbf{B}\perp\mathbf{C}$. Then we extend this approach to the case of resonant LH states, and demonstrate how the resonant energy-level position and level width can be defined. Finally we discuss the influence of the transition from localized to resonant states on the electron-LH optical transitions and other phenomena.

BASIC EQUATIONS

We analyze the resonant hole states in a single QW with DMS barriers using the following simplest model, which allow us to find an exact solution of Luttinger equation.

(i) A hole under consideration is localized in a nonmagnetic QW with symmetric rectangular DMS barriers with sharp interfaces. For definiteness, the growth axis is directed along $\mathbf{C}\|[100]$. We do not consider the interface effects here, which, however, are important for a DMS QW under these conditions (Refs. 9–11). Thus, the potential and exchange field profiles along the growth axis (*x* axis) have the forms

$$U_h(x)=\begin{cases}0, & |x|<L_W/2\\ U_h, & |x|>L_W/2,\end{cases}\quad \mathbf{G}_h(x)=\begin{cases}0, & |x|<L_W/2\\ \mathbf{G}_h, & |x|>L_W/2,\end{cases} \tag{1}$$

where zero energy corresponds to the QW bottom.

(ii) The magnetic field does not affect the hole kinetic energy. The influence of the magnetic field **B** reduces to the induction of the exchange field $\mathbf{G}_h$ only.

(iii) The strain effect as well as any excitonic effects is beyond the framework of consideration. Thus, it is assumed that the localization of a hole is provided due to the band-offset potential and exchange interaction only.

(iv) The influence of the spin-orbit-split subband Γ_7 is negligible. So we use the Luttinger equation (LE) to describe the hole states.

(v) We consider HH and LH ground states with zero in-plane wave vectors only.

The aforementioned assumptions permit us to write the Hamiltonian in terms of angular momentum **J**. It is also convenient to rewrite the LE in dimensionless variables introducing the length unit L_W and the energy unit $E_0=\hbar^2/2m_0L_W^2$, where L_W is the QW width and m_0 the free-electron mass. We direct the $\mathbf{B}\perp\mathbf{C}$ and put the *OX* and *OZ* axes along **C** and **B** directions, respectively. In these units the Hamiltonian assumes the form

$$\hat{H}_L=(\gamma_1+\tfrac{5}{2}\gamma_2)k_X^2-2\gamma_2J_X^2k_X^2-\tfrac{1}{3}g_h(\xi)J_Z+u(\xi), \tag{2}$$

where $u(\xi)=U_h/E_0$, $g(\xi)=G_h/E_0$, $\xi=x/L_W$, and $k_X=-i\partial/\partial\xi$, and γ_1 and γ_2 are Luttinger parameters. Here we took into account the negative (antiferromagnetic) sign of hole exchange constant β that leads to the negative *Z*-projection of the exchange field $\mathbf{G}_h$: $G_{hZ}=-G_h$, where $G_h=|\mathbf{G}_h|$.

The 4×4 matrix of the Luttinger Hamiltonian in the space of eigenvectors of the J_Z operator breaks up into two 2×2 submatrices for $(\pm\frac{3}{2}, \mp\frac{1}{2})$ subspaces (Ref. 11). For the $(+\frac{3}{2}, -\frac{1}{2})$ subspace the matrices of Hamiltonian for the barrier (*B*) and well (*W*) regions have the forms

$$\hat{H}_B=\begin{pmatrix}-(\gamma_1+\gamma_2)\dfrac{\partial^2}{\partial\xi^2}-\dfrac{g}{2}+u & \sqrt{3}\gamma_2\dfrac{\partial^2}{\partial\xi^2}\\ \sqrt{3}\gamma_2\dfrac{\partial^2}{\partial\xi^2} & -(\gamma_1-\gamma_2)\dfrac{\partial^2}{\partial\xi^2}+\dfrac{g}{6}+u\end{pmatrix}, \tag{3}$$

$$\hat{H}_W=\begin{pmatrix}-(\gamma_1+\gamma_2)\dfrac{\partial^2}{\partial\xi^2} & \sqrt{3}\gamma_2\dfrac{\partial^2}{\partial\xi^2}\\ \sqrt{3}\gamma_2\dfrac{\partial^2}{\partial\xi^2} & -(\gamma_1-\gamma_2)\dfrac{\partial^2}{\partial\xi^2}\end{pmatrix}. \tag{4}$$

Matrices of the Hamiltonian for the $(-\frac{3}{2}, +\frac{1}{2})$ subspace are obtained from Eqs. (3) and (4) by replacing g with $-g$.

Corresponding wave functions for each subsystem have the form $\Psi(x)=\theta(L_W/2-|x|)\Psi^W(x)+\theta(|x|-L_W/2)\Psi^B(x)$, where $\theta(x)$ is Heaviside (unit step) function. $\Psi^W(x)$ and $\Psi^B(x)$ are the two-component eigenfunctions of Hamiltonians (4) and (3), respectively,

$$\Psi^W=\begin{pmatrix}\Psi_h^W\\ \Psi_l^W\end{pmatrix},\quad \Psi^B=\begin{pmatrix}\Psi_h^B\\ \Psi_l^B\end{pmatrix}, \tag{5}$$

where $h=\pm\frac{3}{2}$ and $l=\mp\frac{1}{2}$.

The solutions of the LE with Hamiltonian $\hat{H}=\theta(|x|-L_W/2)\hat{H}_B+\theta(L_W/2-|x|)\hat{H}_W$ are exponential functions $\Psi^W(x)=A^W\exp(ikx)$ and $\Psi^B(x)=A^B\exp(\lambda x)$, where A^W and A^B are the two-component numerical vectors. Generally,

there are four k_j and λ_j satisfying LE's with Hamiltonians (3) and (4), respectively. So we can write

$$\Psi^W=\sum_{j=1,2,3,4} A_j^W \exp(ik_j\xi), \quad \Psi^B=\sum_{j=1,2,3,4} A_j^B \exp(\lambda_j\xi), \tag{6}$$

with

$$k_{1,3}=\pm\left(\frac{\varepsilon}{\gamma_1+2\gamma_2}\right)^{1/2}, \quad k_{2,4}=\pm\left(\frac{\varepsilon}{\gamma_1-2\gamma_2}\right)^{1/2}, \tag{7}$$

$$\lambda_{1,3}=\pm\left(\frac{\gamma_1\delta+\gamma_2\frac{g}{3}+\rho}{\gamma_1^2-4\gamma_2^2}\right)^{1/2},$$

$$\lambda_{2,4}=\pm\left(\frac{\gamma_1\delta+\gamma_2\frac{g}{3}-\rho}{\gamma_1^2-4\gamma_2^2}\right)^{1/2}, \tag{8}$$

where

$$\rho=\left((2\gamma_2\delta)^2+(\gamma_1^2-3\gamma_2^2)\frac{g^2}{9}+2\gamma_1\gamma_2\delta\frac{g}{3}\right)^{1/2},$$

$$\delta=u-\varepsilon-g/6. \tag{9}$$

Parameters $A_j^{W(B)}$ and energy ε should be found from the LE, boundary conditions, and normalization condition for the Ψ function. All coefficients k_j [Eq. (7)] as well as square root ρ [Eq. (9)] are real because $\gamma_1>2\gamma_2$, while λ_j can be both real and imaginary. The conditions for λ_j to be real follow from Eqs. (8), and have the form $u-\varepsilon>g/2$ for the basis of $(+\frac{3}{2}, -\frac{1}{2})$ and $u-\varepsilon>g/6$ for the basis of $(-\frac{3}{2}, +\frac{1}{2})$. One can see (Fig. 1) that just these inequalities satisfy the requirement for energy to be separated from the continuous barrier spectrum. We emphasize that the appearance of two inequalities is the result of reduction of the 4×4 Hamiltonian matrix into two 2×2 matrices in the case of $\mathbf{B}\perp\mathbf{C}$. Generally speaking, the first condition provides all λ_j to be real.

Subsequent calculations essentially depend on the boundary conditions far from the interface. So the localized (all λ_j are real) and extended (some of λ_j are imaginary) solutions of the LE will be considered separately. For numerical calculations throughout this paper we used the parameters corresponding to $Cd_{0.88}Mn_{0.12}Te/CdTe/Cd_{0.88}Mn_{0.12}Te$ 20-Å-wide QW with a valence-band offset of $Q=0.4$.[12,13] This gives the barrier height for holes $u_h=7.87$ (in E_0 units). Luttinger parameters are chosen to be equal to $\gamma_1=5.3$ and $\gamma_2=1.62$.

DISCRETE SPECTRUM

Let us consider the energy range corresponding to the real values of λ_j [Eq. (8)], i.e.,

$$\Delta^2>(G/3)^2, \tag{10}$$

where $\Delta=E_0\delta$. Inequality (10) results in the condition $E<U-G/2$ for the $(+\frac{3}{2},-\frac{1}{2})$ subsystem or $E<U-G/6$ for the $(-\frac{3}{2},+\frac{1}{2})$ subsystem. These inequalities have a clear physical meaning: the eigenenergies of localized states in the QW should be lower than the continuous barrier states far from the QW region with effective spin projections $+\frac{3}{2}$ and $+\frac{1}{2}$, respectively.

Thus the parameters k_j [Eq. (7)] and λ_j [Eq. (8)] are real and positive. So the spinor components of the wave function have cosine or sine behaviors inside the well, and decay exponentially in the barrier. Since we consider only the ground state, corresponding wave functions for the symmetrical potential should be even. In this case Eqs. (5) and (6) can be rewritten in the following form:

$$\Psi^W(\xi)=\begin{pmatrix}\Psi_h^W\\ \Psi_l^W\end{pmatrix}=\begin{pmatrix}W_{h1}\\ W_{l1}\end{pmatrix}\cos(k_1\xi)+\begin{pmatrix}W_{h2}\\ W_{l2}\end{pmatrix}\cos(k_2\xi),$$

$$\Psi^B(\xi)=\begin{pmatrix}\Psi_h^B\\ \Psi_l^B\end{pmatrix}=\begin{pmatrix}B_{h1}\\ B_{l1}\end{pmatrix}\exp(-\lambda_1|\xi|)+\begin{pmatrix}B_{h2}\\ B_{l2}\end{pmatrix}\exp(-\lambda_2|\xi|), \tag{11}$$

where the boundary conditions $|\Psi|^2 \xrightarrow[x\to\pm\infty]{} 0$ are taken into account.

The relations between HH and LH components of Ψ functions (11) are obtained from LE's with Hamiltonians (3) and (4):

$$W_{li}=C_{Wi}W_{hi},$$

$$B_{li}=C_{Bi}B_{hi}, \quad i=1,2, \tag{12}$$

with coefficients

$$C_{Wi}=\frac{(\gamma_1+\gamma_2)k_i^2-\varepsilon}{\sqrt{3}\gamma_2 k_i^2},$$

$$C_{Bi}=-\frac{-(\gamma_1+\gamma_2)\lambda_i^2+\frac{g}{2}+u-\varepsilon}{\sqrt{3}\gamma_2\lambda_i^2}. \tag{13}$$

The remaining four unknown components W_{h1}, W_{h2}, B_{h1}, and B_{h2} are found from the set of four linear homogeneous equations, which stem from the continuity conditions on the interface:

$$\lim_{\zeta\to1/2-0}\psi_W=\lim_{\zeta\to1/2+0}\psi_B,$$

$$\lim_{\xi\to1/2-0}\hat{V}\Psi_W=\lim_{\xi\to1/2+0}\hat{V}\Psi_B, \tag{14}$$

where

$$\hat{V}=\begin{pmatrix}-(\gamma_1+\gamma_2)\frac{\partial}{\partial\xi} & \sqrt{3}\gamma_2\frac{\partial}{\partial\xi}\\ \sqrt{3}\gamma_2\frac{\partial}{\partial\xi} & -(\gamma_1-\gamma_2)\frac{\partial}{\partial\xi}\end{pmatrix}. \tag{15}$$

The equating of corresponding determinant to zero leads to a transcendental equation for the energies ε_i. The explicit form of the initial system is presented in Appendix A [Eqs. A1].

A numerical solution of the transcendental equation for each of the two subsystems gives at least two roots for each

value of the exchange field G satisfying condition (10). One of them corresponds to the HH state, while the other corresponds to the LH state. The example of the magnetic-field dependence of HH and LH energies is shown in Fig. 1 [solid lines correspond to the $(-\frac{3}{2},+\frac{1}{2})$ subsystem and dashed lines to the $(+\frac{3}{2},-\frac{1}{2})$ system]. One can see that LH branches break at exchange field values violating conditions (10).

CONTINUOUS SPECTRUM

At large enough values of **G** condition (10) is no longer satisfied, so that $\lambda_{2,4}$ in Eq. (8) become imaginary. This corresponds to the appearance of the nonvanishing periodic part in the barrier function $\Psi^B(x)$ in Eq. (6). In this case the boundary condition $|\Psi|^2 \xrightarrow[x\to\pm\infty]{} 0$ is no longer valid, which means that coefficients A_2^B and A_4^B in Eq. (6) are not zero. So one can write the following expression for the wave function in the barrier instead of Eq. (11):

$$\Psi^B(\xi)=\begin{pmatrix}\Psi_h^B\\ \Psi_l^B\end{pmatrix}=\begin{pmatrix}B_{h1}\\ B_{l1}\end{pmatrix}\exp(-\lambda_1|\xi|)+\begin{pmatrix}B_{h2}\\ B_{l2}\end{pmatrix}\cos(q|\xi|+\varphi). \tag{16}$$

Here we introduce the wave vector in the barrier $q=-i\lambda_2$ and phase φ. Contrary to the case of localized states, we do not need to determine the eigenenergy. Rather, we shall find phase φ and other parameters of the Ψ function at a given energy value.

We still limit consideration to even solutions of the LE only. The reason for this is that only even hole states contribute to optical transitions between the hole states and the electron ground state which are under consideration.

Equation (16) clearly shows peculiarities of the hole states in a single QW with semimagnetic barriers. That is, the hole state is now defined as a superposition of localized (first term) and delocalized (second term) hole states. The relative values of the corresponding coefficients represent their partial contributions to eigenstate.

The following calculations are very similar to those for the discrete spectrum. The analog of Eq. (13), however, is different:

$$C_{B2}=-\frac{(\gamma_1+\gamma_2)q^2+\dfrac{g}{2}+u-\varepsilon}{\sqrt{3}\gamma_2 q^2}. \tag{17}$$

The continuity conditions (14) on the interface lead to a set of four homogeneous algebraic equations [see Appendix A, Eqs. (A2)]. Equating the corresponding determinant to zero now gives the transcendental equation for phase φ as a function of energy ε and exchange field g.

To complete the determination of the wave functions, we need to normalize them. The most convenient and proper way is to introduce the crystal size in the x direction $L\gg 1$ (in L_W units) and normalize the integral of the wave function density:

$$\int_{-L/2}^{L/2}|\Psi|^2 d\xi=1. \tag{18}$$

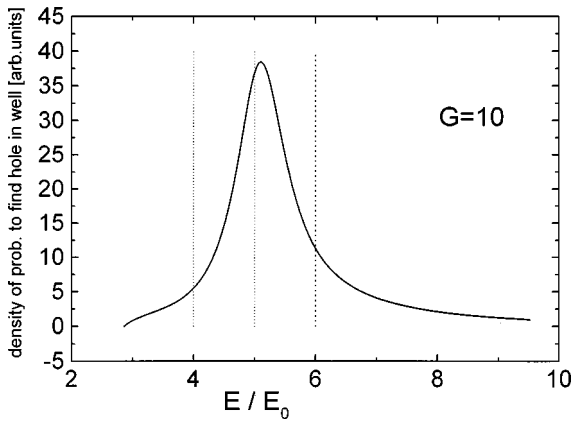

FIG. 2. Density of probability to find a hole in the QW region as a function of the hole energy, calculated for the $(+\frac{3}{2},-\frac{1}{2})$ subsystem in a 20-Å-wide $Cd_{0.88}Mn_{0.12}Te/CdTe/Cd_{0.88}Mn_{0.12}Te$ QW for the value of the exchange field $G=10$ (compare with Fig. 1). The sense of the vertical lines is disclosed in Fig. 3.

Simple calculations reduce the normalization condition (18) to the equation

$$\begin{aligned}\int_{-L/2}^{L/2}|\Psi|^2 d\xi&=\int_{-1/2}^{1/2}|\Psi^W|^2 d\xi+2\int_{1/2}^{L/2}|\Psi^B|^2 d\xi\\ &=2(B_{h2}^2+B_{l2}^2)\int_0^{L/2}\cos^2(q\xi+\varphi)d\xi+O\left(\frac{1}{L}\right)\\ &=\frac{L}{2}B_{h2}^2(1+C_{B2}^2)+O\left(\frac{1}{L}\right)=1,\end{aligned}$$

that gives, in the limit $L\gg 1$,

$$B_{h2}^2=\frac{2}{L}\frac{1}{1+C_{B2}^2}. \tag{19}$$

To determine parameters of the wave function, one can obtain the system of three linear algebraic equations from Eqs. (19) and (14) (Appendix B). We plot the results of the wave-function calculations in Figs. 2 and 3. The probability to find hole in the well region $\int_{-1/2}^{+1/2}|\Psi|^2 d\xi$ as a function of hole energy ε demonstrates a nonmonotonic behavior with the maximum at some energy ε_0 and width Γ (see Fig. 2). This can be associated with the energy ε_0 and lifetime $\hbar/\Gamma$ of the resonant (virtual) level. Figure 3 shows the explicit form of the hole wave function at $\varepsilon<\varepsilon_0$ (a) and $\varepsilon>\varepsilon_0$ (c), and at a resonant value ε_0 (b).

The resonant energies ε_0 as a function of exchange field g are plotted in Fig. 1 (symbols). The bars correspond to the full width at half maximum of the curves in Fig. 2. Width Γ for the LH virtual level from subsystem $(-\frac{3}{2},+\frac{1}{2})$ is larger than that for the LH virtual level from the $(+\frac{3}{2},-\frac{1}{2})$ subsystem. This is not surprising because LH states in the QW and in the barrier are characterized by stronger interaction than LH-HH ones. Width Γ is increased with distance from the point of the localized-resonant transition, i.e., the width $\Gamma(g=8)>\Gamma(g=6)$ (see Fig. 1). Note also that energies ε_0 provide a continuous transition between localized and resonant ''phases'' in terms of the energy-level position.

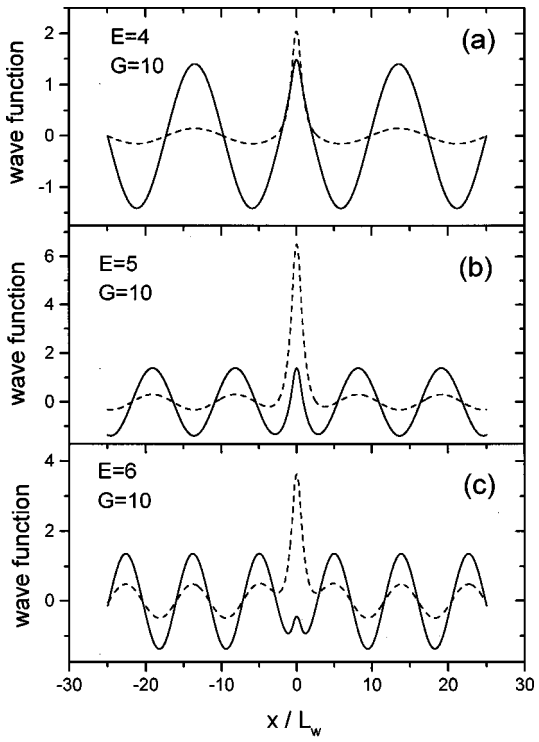

FIG. 3. Two-component wave functions calculated at $\varepsilon<\varepsilon_0$ (a), $\varepsilon>\varepsilon_0$ (c) and at resonant energy ($\varepsilon=\varepsilon_0$) (b) for parameters similar to those in Fig. 2. Solid lines correspond to the HH component of the wave function, while dotted lines correspond to the LH component. The energies correspond to the positions of vertical lines in Fig. 2.

OPTICAL TRANSITIONS

Among the different manifestations of the considered hole transformation, we choose the interband optical transition as a phenomenon sensitive to the transition from confinement to resonant hole states. In addition there are experimental data (see Refs. 9 and 13) on GSS, which should be treated in regard to the possibility of resonant dissociation of excitons to a bound electron and a free hole due to LH-HH mixing by a strong enough magnetic field directed in the plane of the QW. For the sake of simplicity, we now consider optical transitions without any excitonic effects to retrace the transition through a critical value G_c in terms of the theory developed above.

Let us consider the probabilities of electron-hole optical transitions between the considered hole states and the ground state of the conduction electron in a QW. The shape and width of the corresponding optical line in the energy range of the continuous hole spectrum reflect the probability of finding a hole in the QW region, and are similar to the shape and width of the curve in Fig. 2. In the energy range of the discrete hole spectrum, the optical transition probabilities are described by δ functions. At the same time, the integral intensity can be calculated and compared for both discrete and continuous spectra.

So we consider the probability of optical transitions between localized electron and LH states:

$$P(E)=\sum_f \frac{2\pi}{\hbar}|M_{fi}|^2\delta(E_f-E_i-E). \tag{20}$$

Here E_i is the electron ground-state energy in a QW, and E_f is the LH energy depending on space (q) and spin (σ) quantum numbers. M_{fi} is proportional to $\boldsymbol{\varepsilon}\mathbf{p}_{fi}$ where $\boldsymbol{\varepsilon}$ and $\mathbf{p}_{fi}$ are the polarization vector of light and momentum matrix element. The detailed calculation of the matrix element $\mathbf{p}_{fi}$ is performed in Appendix C. The expression

$$I=\int_{E_{\min}}^{E_{\max}}P(E)dE \tag{21}$$

can be applied to a calculation of the integral intensities we are interested in. In the case of the continuous hole spectrum, the lower and upper limits of integration in Eq. (21) should be chosen far enough from the intensity maximum.

In the case of the discrete hole spectrum, the calculations give the following values of integral intensities for π and σ polarizations:

$$I_\pi=\frac{2\pi}{\hbar}\frac{4}{6}|\langle S|p_\pi|Z\rangle|^2|\langle\Psi_e|\Psi_l^W\rangle|^2,$$

$$I_\sigma=\frac{2\pi}{\hbar}|\langle S|p_\sigma|Y\rangle|^2\left|\frac{1}{\sqrt{2}}\langle\Psi_e|\Psi_h^W\rangle+\frac{1}{\sqrt{6}}\langle\Psi_e|\Psi_l^W\rangle\right|^2. \tag{22}$$

Here Ψ_e is a confinement electron wave function.

The case of the continuous spectrum is considered in the usual fashion by integration (instead of summation) with a one-dimensional density of states $\rho(q)=L/2\pi$:

$$I(E)=\sum_\sigma\frac{L}{\hbar}\int_{E_{\min}}^{E_{\max}}|p_{fi}|^2\delta(E_f-E_i-E)\frac{\partial q}{\partial E_f}dE_f. \tag{23}$$

The derivative $\partial q/\partial E_f$ can be obtained by direct differentiation of Eq. (8) with respect to the relation $q=-i\lambda_2$. The integration limit $E_{\min}$ is also determined by the condition opposite to inequality (10). Thus one can obtain

$$I(\varepsilon)=\sum_\sigma\frac{L}{\hbar}\frac{\partial q(E_i=\varepsilon)}{\partial E_i}|p_{fi}(E_i=\varepsilon)|^2, \tag{24}$$

where $\varepsilon=E_i-E$, and the energy of optical perturbation $E=\hbar\omega$. Therefore, the integral intensities of the optical transitions in the case of continuous hole spectrum have the forms

$$I_\pi=\frac{4}{3\hbar}|\langle S|p_Z|Z\rangle|^2\times\int_{\varepsilon_{\min}}^{\varepsilon_{\max}}\frac{\partial q(\varepsilon)}{\partial E_i}|\langle\Psi_e|\Psi_l^W(\varepsilon)\rangle|^2\frac{1}{1+C_{b2}^2(\varepsilon)}d\varepsilon,$$

$$I_\sigma=\frac{2}{\hbar}|\langle S|p_Y|Y\rangle|^2\int_{\varepsilon_{\min}}^{\varepsilon_{\max}}\frac{\partial q(\varepsilon)}{\partial E_i}\times\left|\frac{1}{\sqrt{2}}\langle\Psi_e|\Psi_h^W(\varepsilon)\rangle+\frac{1}{\sqrt{6}}\langle\Psi_e|\Psi_l^W(\varepsilon)\rangle\right|^2\times\frac{1}{1+C_{b2}^2(\varepsilon)}d\varepsilon. \tag{25}$$

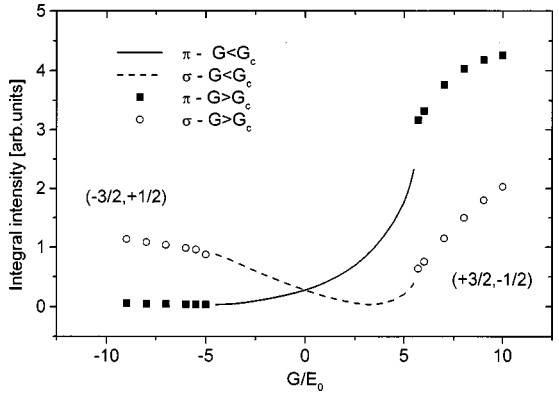

FIG. 4. Integral intensities of the optical transitions between LH states and ground electron state in the 20-Å-wide $Cd_{0.88}Mn_{0.12}Te/CdTe/Cd_{0.88}Mn_{0.12}Te$ QW as functions of the exchange field $\mathbf{G}\perp\mathbf{C}$. Negative values of G correspond to the $(-\frac{3}{2},+\frac{1}{2})$ subsystem, while positive G corresponds to the $(+\frac{3}{2},-\frac{1}{2})$ subsystem. The solid line and square symbols correspond to π polarizations, in the regions $G<G_c$ and $G>G_c$, respectively. The dashed line and open circles correspond to σ polarization.

Figure 4 shows the dependence of the integral intensities of the electron-LH optical transitions on the exchange field G. Symbols correspond to transitions involving the continuous hole spectrum in the range of $G>G_c$ [Eqs. (25)]. Integral intensities in the case of $G<G_c$ are presented in Fig. 4 by lines. Note, that the significant redistribution of the oscillator strength between transitions from discrete and continuous hole spectra takes place in the vicinity of the critical exchange field G_c. On the other hand, both discrete [Eqs. (22)] and continuous [Eqs. (25)] spectra should contribute to the optical line if the energy distance between them is about the same as or smaller than the linewidth. Thus our calculations of the integral intensity presented in Fig. 4 involve both types of transitions. One can see that the integral intensities demonstrate a smooth continuation from the region of localized ($G<G_c$) states to the region of resonant ($G>G_c$) states. Therefore, the optical linewidths should reveal additional homogeneous broadening in the region of $G>G_c$ without a significant change of integral intensity.

CONCLUSION

This work shows that along with localized and delocalized hole states, single quantum well can also possess an intermediate state consisting of their superposition if the barriers are semimagnetic and the external magnetic field is strong enough and inclined toward the growth axis **C**. In Fig. 5 we plot the values of critical magnetic fields B_{c1} and B_{c2} for $Cd_{1-x}Mn_xTe/CdTe/Cd_{1-x}Mn_xTe$ QW structures as functions of molar concentration of the Mn-ions in the barriers for different values of well widths. One can see that, for the majority of commonly used structures, these critical fields can be easily reached experimentally.

The considered model allows us to solve the problem without any small parameter in the spirit of calculations of the discrete spectrum with rectangular potential. The probability of finding a hole in the QW region has a resonantlike distribution with a clear maximum. Positions of the maxima are smooth extensions of the localized LH branches to the

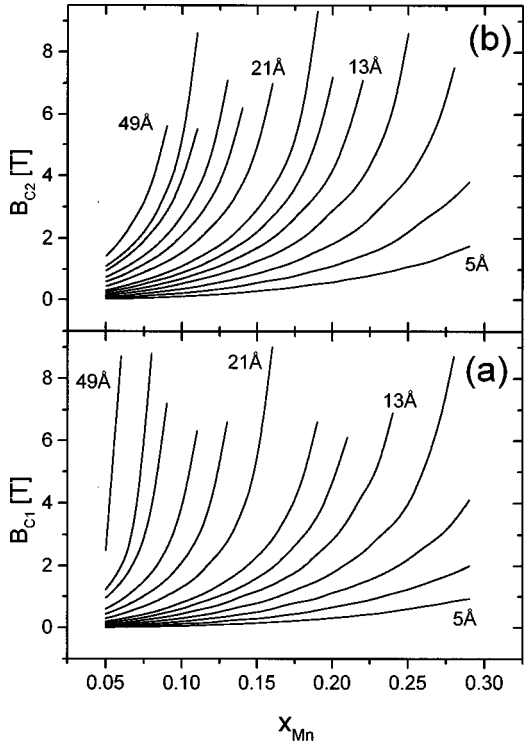

FIG. 5. Critical magnetic fields B_{c1} (a) for the $(-\frac{3}{2},+\frac{1}{2})$ subsystem and B_{c2} (b) for the $(+\frac{3}{2},-\frac{1}{2})$ subsystem as functions of molar concentration of the Mn ions in the barriers for $Cd_{1-x}Mn_xTe/CdTe/Cd_{1-x}Mn_xTe$ QW structures at $T=1.8$ K. Curves correspond to the different values of the well width: 5, 7, 9, 11, 13, 15, 17, 21, 25, 29, 35, 39, and 49 Å. The valence-band-offset parameter is taken to be equal to 0.4.

region where $G>G_c$. The width of this distribution can be associated with the probability for the hole to drain to infinity. Thus we expect that the measurements of the giant spin splitting of LH energies in the Voight configuration will have a smooth continuation from discrete to resonant states. The intensities of the optical transitions are also expected to demonstrate a smooth continuation. In the case of relatively small fluctuations, the widths of resonant levels can be associated with a homogeneous broadening of the optical line in the region of the transition from a localized states regime to a resonant state regime.

Another manifestation of resonant states is expected to be the kinetics of luminescence in QW's when the hole tunneling to infinity (far from the QW) can play the role of an additional channel for subsequent relaxation. In a similar manner, we expect the appearance of peculiarities in the transport properties of such structures. These problems, along with a detailed comparison with experiment (see, for instance, Refs. 13 and 14), will be published elsewhere.

ACKNOWLEDGMENTS

We wish to thank J. Kossut for a critical reading of the manuscript, and S. M. Ryabchenko for helpful discussions.

APPENDIX A

The system of equations for the coefficients W_{h1}, W_{h2}, B_{h1}, and B_{h2}, stemming from Eqs. (14) and (15) assumes the forms

$$
\begin{aligned}
&B_{h1}\exp\left(-\frac{\lambda_1}{2}\right)+B_{h2}\exp\left(-\frac{\lambda_2}{2}\right)-W_{h1}\cos\left(\frac{k_1}{2}\right)-W_{h2}\cos\left(\frac{k_2}{2}\right)=0,\\
&B_{h1}C_{B1}\exp\left(-\frac{\lambda_1}{2}\right)+B_{h2}C_{B2}\exp\left(-\frac{\lambda_2}{2}\right)-W_{h1}C_{W1}\cos\left(\frac{k_1}{2}\right)-W_{h2}C_{W2}\cos\left(\frac{k_2}{2}\right)=0,\\
&B_{h1}[(\gamma_1+\gamma_2)-C_{B1}\sqrt{3}\gamma_2]\lambda_1\exp\left(-\frac{\lambda_1}{2}\right)+B_{h2}[(\gamma_1+\gamma_2)-C_{B2}\sqrt{3}\gamma_2]\lambda_2\exp\left(-\frac{\lambda_2}{2}\right)\\
&\quad-W_{h1}[(\gamma_1+\gamma_2)-C_{W1}\sqrt{3}\gamma_2]k_1\sin\left(\frac{k_1}{2}\right)-W_{h2}[(\gamma_1+\gamma_2)-C_{W2}\sqrt{3}\gamma_2]k_2\sin\left(\frac{k_2}{2}\right)=0,\\
&B_{h1}[-\sqrt{3}\gamma_2+C_{B1}(\gamma_1-\gamma_2)]\lambda_1\exp\left(-\frac{\lambda_1}{2}\right)+B_{h2}[-\sqrt{3}\gamma_2+C_{B2}(\gamma_1-\gamma_2)]\lambda_2\exp\left(-\frac{\lambda_2}{2}\right)\\
&\quad+W_{h1}[\sqrt{3}\gamma_2-C_{B3}(\gamma_1-\gamma_2)]k_1\sin\left(\frac{k_1}{2}\right)+W_{h2}[\sqrt{3}\gamma_2-C_{B4}(\gamma_1-\gamma_2)]k_2\sin\left(\frac{k_2}{2}\right)=0.
\end{aligned}
\tag{A1}
$$

The transcendental equation with respect to the eigenenergy ε is found by equating the determinant of system (A1) to zero. Numerical solution of this equation with respect to ε gives at least two roots associated with HH and LH states. To find the components of corresponding wave functions, the normalization conditions should also be taken into account.

The system of four linear homogenous algebraic equations used for the determination of phase φ as a function of energy ε in the case of continuous spectrum has the forms

$$
\begin{aligned}
&B_{h1}\exp\left(-\frac{\lambda_1}{2}\right)+B_{h2}\cos\left(\frac{q}{2}+\varphi\right)-W_{h1}\cos\left(\frac{k_1}{2}\right)-W_{h2}\cos\left(\frac{k_2}{2}\right)=0,\\
&B_{h1}C_{B1}\exp\left(-\frac{\lambda_1}{2}\right)+B_{h2}C_{B2}\cos\left(\frac{q}{2}+\varphi\right)-W_{h1}C_{W1}\cos\left(\frac{k_1}{2}\right)-W_{h2}C_{W2}\cos\left(\frac{k_2}{2}\right)=0,\\
&B_{h1}[(\gamma_1+\gamma_2)-C_{B1}\sqrt{3}\gamma_2]\lambda_1\exp\left(-\frac{\lambda_1}{2}\right)+B_{h2}[(\gamma_1+\gamma_2)-C_{B2}\sqrt{3}\gamma_2]q\sin\left(\frac{q}{2}+\varphi\right)\\
&\quad-W_{h1}[(\gamma_1+\gamma_2)\ -C_{W1}\sqrt{3}\gamma_2]k_1\sin\left(\frac{k_1}{2}\right)-W_{h2}[(\gamma_1+\gamma_2)-C_{W2}\sqrt{3}\gamma_2]k_2\sin\left(\frac{k_2}{2}\right)=0,\\
&B_{h1}[-\sqrt{3}\gamma_2+C_{B1}(\gamma_1-\gamma_2)]\lambda_1\exp\left(-\frac{\lambda_1}{2}\right)+B_{h2}[-\sqrt{3}\gamma_2+C_{B2}(\gamma_1-\gamma_2)]q\sin\left(\frac{q}{2}+\varphi\right)\\
&\quad+W_{h1}[\sqrt{3}\gamma_2-C_{B3}(\gamma_1-\gamma_2)]k_1\sin\left(\frac{k_1}{2}\right)+W_{h2}[\sqrt{3}\gamma_2-C_{B4}(\gamma_1-\gamma_2)]k_2\sin\left(\frac{k_2}{2}\right)=0.
\end{aligned}
\tag{A2}
$$

APPENDIX B

The system of equations for the coefficients B_{h1}, W_{h1}, and W_{h2} takes the form

$$
\begin{pmatrix}
\exp\left(-\frac{\lambda_1}{2}\right) & -\cos\left(\frac{k_1}{2}\right) & \cos\left(\frac{k_2}{2}\right)\\
C_{B1}\exp\left(-\frac{\lambda_1}{2}\right) & -C_{W1}\cos\left(\frac{k_1}{2}\right) & -C_{W2}\cos\left(\frac{k_2}{2}\right)\\
[\gamma_{12}-C_{B1}\sqrt{3}\gamma_2]\lambda_1\exp\left(-\frac{\lambda_1}{2}\right) & -[\gamma_{12}-C_{W1}\sqrt{3}\gamma_2]k_1\sin\left(\frac{k_1}{2}\right) & -[\gamma_{12}-C_{W2}\sqrt{3}\gamma_2]k_2\sin\left(\frac{k_2}{2}\right)
\end{pmatrix}
\begin{pmatrix} B_{h1}\\ W_{h1}\\ W_{h2}\end{pmatrix}
$$

$$
=\begin{pmatrix}
-\left(\frac{2}{L}\frac{1}{1+C_{B2}^2}\right)^{1/2}\cos\left(\frac{q}{2}+\varphi\right)\\
-\left(\frac{2}{L}\frac{1}{1+C_{B2}^2}\right)^{1/2}C_{B2}\cos\left(\frac{q}{2}+\varphi\right)\\
-\left(\frac{2}{L}\frac{1}{1+C_{B2}^2}\right)^{1/2}[\gamma_{12}-C_{B2}\sqrt{3}\gamma_2]q\sin\left(\frac{q}{2}+\varphi\right)
\end{pmatrix}.
\tag{B1}
$$

Here $\gamma_{12}=\gamma_1+\gamma_2$.

APPENDIX C

For simplicity, the electron envelope function is chosen to be localized in the well region

$$\Psi_c=\sqrt{2}\cos(\pi x). \tag{C1}$$

Basis hole wave functions are determined by the transformation properties of the angular momentum $\frac{3}{2}$ (Ref. 15):

$$\left|\frac{2}{3},+\frac{3}{2}\right\rangle=\frac{1}{\sqrt{2}}(X+iY)\uparrow,$$

$$\left|\frac{3}{2},+\frac{1}{2}\right\rangle=\frac{1}{\sqrt{6}}[(X+iY)\downarrow-2Z\uparrow],$$

$$\left|\frac{3}{2},-\frac{1}{2}\right\rangle=\frac{1}{\sqrt{6}}[-(X-iY)\uparrow-2Z\downarrow],$$

$$\left|\frac{3}{2},-\frac{3}{2}\right\rangle=-\frac{1}{\sqrt{2}}(X-iY)\downarrow. \tag{C2}$$

So the calculations of the momentum matrix elements in the basis $(+\frac{3}{2},-\frac{1}{2})$ give, for the π-($\mathbf{e}\|OZ$) and σ-($\mathbf{e}\|OY$) polarizations,

$$|p_\pi^{fi}|^2=\begin{cases}\frac{4}{6}|\langle S|p_Z|Z\rangle|^2|\langle\Psi_e|\Psi_l^W\rangle|^2, & \sigma_e=-\frac{1}{2}\\ 0, & \sigma_e=+\frac{1}{2},\end{cases}$$

$$|p_\sigma^{fi}|^2=\begin{cases}\left|\frac{1}{\sqrt{2}}\langle\Psi_e|\Psi_h^W\rangle+\frac{1}{\sqrt{6}}\langle\Psi_e|\Psi_l^W\rangle\right|^2|\langle S|p_Y|Y\rangle|^2, & \sigma_e=+\frac{1}{2}\\ 0, & \sigma_e=-\frac{1}{2}.\end{cases} \tag{C3}$$

Calculations in the basis $(-\frac{3}{2},+\frac{1}{2})$ result in formula (C3), with an inverse electron-spin projection $\sigma_e\rightarrow-\sigma_e$.

[1] S. M. Ryabchenko, Izv. Akad. Nauk SSSR Ser. Fiz. **46**, 440 (1982) [Bull. Acad. Sci. USSR, Phys. Ser. **46**, 22 (1982)].
[2] B. Kuhn-Heinrich, M. Popp, W. Ossau, E. Bangert, A. Waag, and G. Landwehr, Semicond. Sci. Technol. **8**, 1239 (1993).
[3] J. K. Furdyna, Solid-State Electron. **37**, 1065 (1994).
[4] E. Deleporte, J. M. Berroir, G. Bastard, C. Delalande, J. M. Hong, and L. L. Chang, Phys. Rev. B **42**, 5891 (1990).
[5] D. R. Yakovlev, W. Ossau, G. Landwehr, R. N. Bicknell-Tassius, A. Waag, and I. N. Uraltsev, Solid State Commun. **76**, 325 (1990).
[6] B. Freytag, U. Rössler, and O. Ponkratov, Semicond. Sci. Technol. **8**, S243 (1993).
[7] G. M. Minkov, A. V. Germanenko, V. A. Larionova, and O. E. Rut, Phys. Rev. B **54**, 1841 (1996).
[8] V. A. Larionova and A. V. Germanenko, Phys. Rev. B **55**, 13 062 (1997).
[9] J. A. Gaj, W. Grieshaber, C. Boden-Deshayes, J. Cibert, G. Feuillrt, Y. Merle d'Aubigne, and A. Wasiela, Phys. Rev. B **50**, 5512 (1994).
[10] Yu. G. Semenov, Acta Phys. Pol. A **94**, 526 (1998).
[11] W. Grieshaber, J. Cibert, J. Gaj, Y. Merle d'Aubigne, and A. Wasiela, Phys. Rev. B **50**, 2011 (1994).
[12] M. Kutrowski, T. Wojtowicz, G. Cywinski, G. Karczewski, E. Janik, E. Dynowska, J. Kossut, P. Kossacki, R. Fiederling, A. Pfeuffer-Jeschke, and W. Ossau, Acta Phys. Pol. A **92**, 887 (1997).
[13] J. Siviniant, F. V. Kyrychenko, Y. G. Semenov, D. Coquillat, D. Scalbert, and J. P. Lascaray, Phys. Rev. B **59**, 10 276 (1999).
[14] P. Peyla, A. Wasiela, Y. Merle d'Aubigne, D. E. Ashenford, and B. Lunn, Phys. Rev. B **47**, 3783 (1993).
[15] Yu. G. Semenov and B. D. Shanina, Phys. Status Solidi B **104**, 631 (1981)